Pure Appl. Geophys. 177 (2020), 3761–3774

https://doi.org/10.1007/s00024-020-02479-z

Pure and Applied Geophysics

Spatiotemporal Seismicity Evolution and Seismic Hazard Potentials in the Western East Sea (Sea of Japan)

Tae-Kyung Hong,[1] Seongjun Park,[1] Junhyung Lee,[1] and Woohan Kim[2]

Abstract—The earthquakes in the western East Sea (Sea of Japan) mostly occur in the continental margin off the east coast of the Korean Peninsula. The seismic hazard potentials in and around the western Ease Sea are studied based on analyses of tectonic structures, seismicity features, earthquake source properties, Coulomb stress changes, and strong ground motions. The earthquake source mechanisms suggest that paleo-rifting structures in the western East Sea were activated by the current stress field. A low stress cumulation rate results in the occurrence of earthquakes with long recurrence intervals. The background seismicity suggests that earthquakes with magnitudes M_w 5.0, 6.0, and 7.0 may occur within every ~ 44, ~ 336, and ~ 2550 years at 95 % confidence level. The spatial distribution of earthquakes changes with time. Most earthquakes are clustered within ~ 60 km from the coast. The seismicity analysis indicates an apparent increase of moderate-size (M_w 3–5) earthquakes since the 2011 M_w 9.0 Tohoku-Oki megathrust earthquake. Static stress changes by moderate-size inland earthquakes induce offshore events. The seismicity and Coulomb stress changes suggest high seismic potentials around the western margin of the Ulleung basin. Earthquakes with magnitudes M_w 6.0–7.0 in the western East Sea may produce peak ground accelerations of 0.2 g within the distance of ~ 40–80 km, which includes the coastal regions.

Keywords: Seismic hazard potentials, East Sea, Sea of Japan, strong motion, continental margin, seismicity.

1. Introduction

The 11 March 2011 M_w 9.0 Tohoku-Oki earthquake occurred in the area ~ 1200 km away from the Korean Peninsula. The megathrust earthquake produced distance-dependent coseismic and postseismic displacements, causing medium weakening and stress perturbation in the crust around the Korean Peninsula (Hong et al. 2017a). The seismic velocities in the crust of the Korean Peninsula decreased by ~ 3% instantly after the megathrust earthquake, recovering gradually with time (Hong et al. 2017a). The transitional medium-property and stress-field changes cause seismicity change in the region. The occurrence rate of M5-level earthquakes increased by 4.7 times since the megathrust earthquake (Hong et al. 2018). Recent moderate-size earthquakes including the 12 September 2016 M_w5.4 (M_L 5.8) Gyeongju earthquake and 15 November 2017 M_w5.5 (M_L 5.4) Pohang earthquake produced high seismic damages around the epicentral area (Hong et al. 2017b, 2018). The recent seismicity raised public concerns on seismic hazard potentials around the peninsula.

The East Sea (Sea of Japan) is placed between the Korean Peninsula and Japanese islands (Fig. 1). The East Sea and Korean Peninsula compose the eastern margin of the Eurasian plate that experienced complex tectonic history including continental collision and rifting (Fitches et al. 1991; Yin and Nie 1993; Chough et al. 2000; Kim et al. 2003). The seismicity around the continental margin in the western East Sea is naturally adjacent to the east coast of the Korean Peninsula (Fig. 2). The paleo-rifting structures in the continental margin are major earthquake-spawning sources.

The orientation of the primary compressional stress field changes laterally in the East Sea (Choi et al. 2012; Lee et al. 2017). The paleo-rifting structure responds to the current ambient stress field, producing earthquakes (Choi et al. 2012; Hong and Choi 2012; Hong et al. 2015). Strike-slip earthquakes

[1] Department of Earth System Sciences, Yonsei University, 50 Yonsei-ro, Seodaemun-gu, Seoul 120-749, South Korea. E-mail: tkhong@yonsei.ac.kr
[2] Department of Earth and Environmental Sciences and RINS, Gyeongsang National University, Jinju 660-701 Gyeongsangnam-do, South Korea.

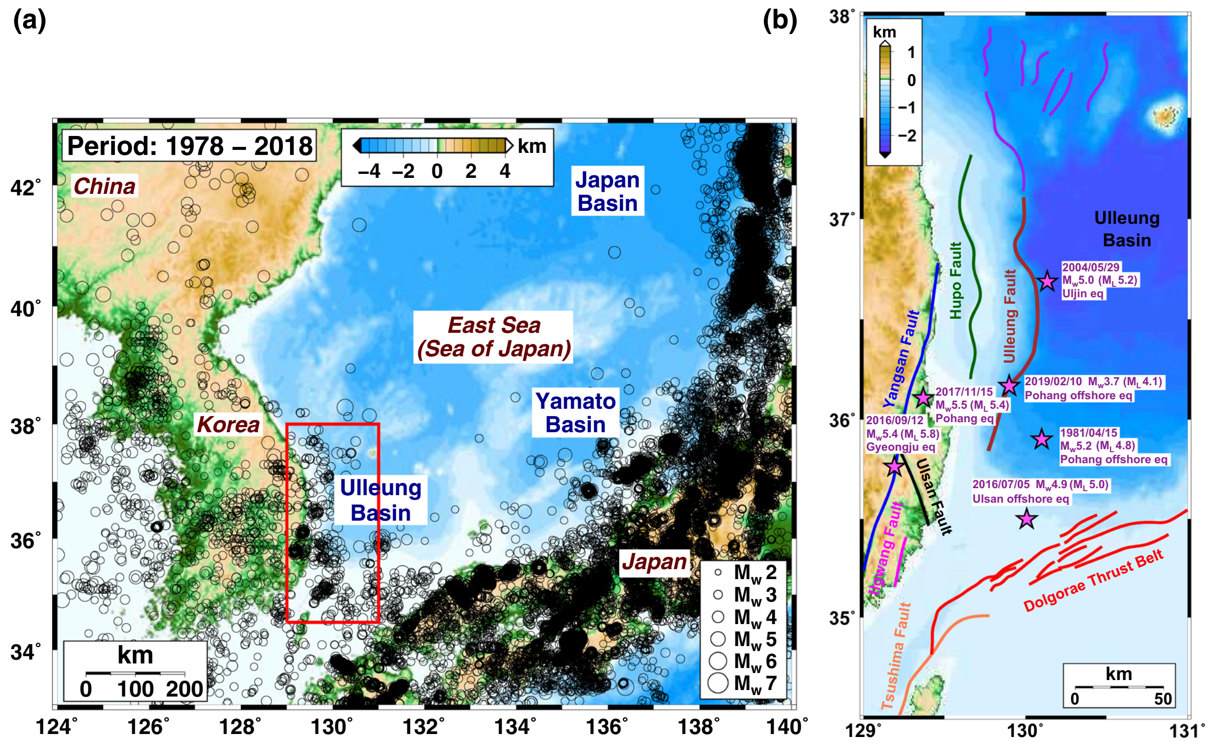

Figure 1

a Seismicity in 1978–2018 in the East Sea (Sea of Japan) and **b** major earthquakes and geological structures around the western East Sea. Major faults around the western East Sea are indicated (Kim et al. 2011; Yoon et al. 2014). Earthquakes mainly occur in inland regions and offshore regions near the coasts

occur along with reverse-faulting events. The source mechanisms of earthquakes are mixed. The interaction and induction of earthquakes between different fault types is poorly understood in the East Sea. The maximum magnitude and earthquake interaction may be associated with the ambient stress field.

The earthquakes around the continental margin may affect the coastal regions where key infrastructures are placed. It is crucial to assess the seismic hazard potentials. We collect all available seismicity records since early 1900. We, finally, determine the maximum magnitude of earthquakes, potential earthquake locations, and expected strong ground motions by large earthquakes. We investigate the properties of earthquakes, and infer the potential locations of large earthquakes. We determine the possible magnitudes of strong motions by potential earthquakes.

2. *Data and Geology*

A continental rifting in Oligocene to mid-Miocene separated the Japanese islands from the Korean Peninsula, opening the East Sea (Otofuji et al. 1985; Jolivet et al. 1994). Three deep-sea basins (Japan, Yamato, and Ulleung basins) underlain by oceanic crust were formed during the paleo-rifting (Hirata et al. 1992; Kim et al. 1998) (Fig. 1). Also, the paleo-rifting developed normal-faulting structures around the margins of basins. The continental shelf between the Ulleung basin and Korean Peninsula displays a transitional structure between continental and oceanic crusts. The crustal thicknesses in the East Sea are 8.5–14 km (Hirata et al. 1992; Kim et al. 1998).

The seismic properties illuminate the paleo-rifting region. Crust-guided shear waves (*Lg*) are blocked in the East Sea. The *Lg* waves are strong in the Korean Peninsula where continental crusts are present (Hong 2010; Furumura et al. 2014; Hong et al. 2016a). The

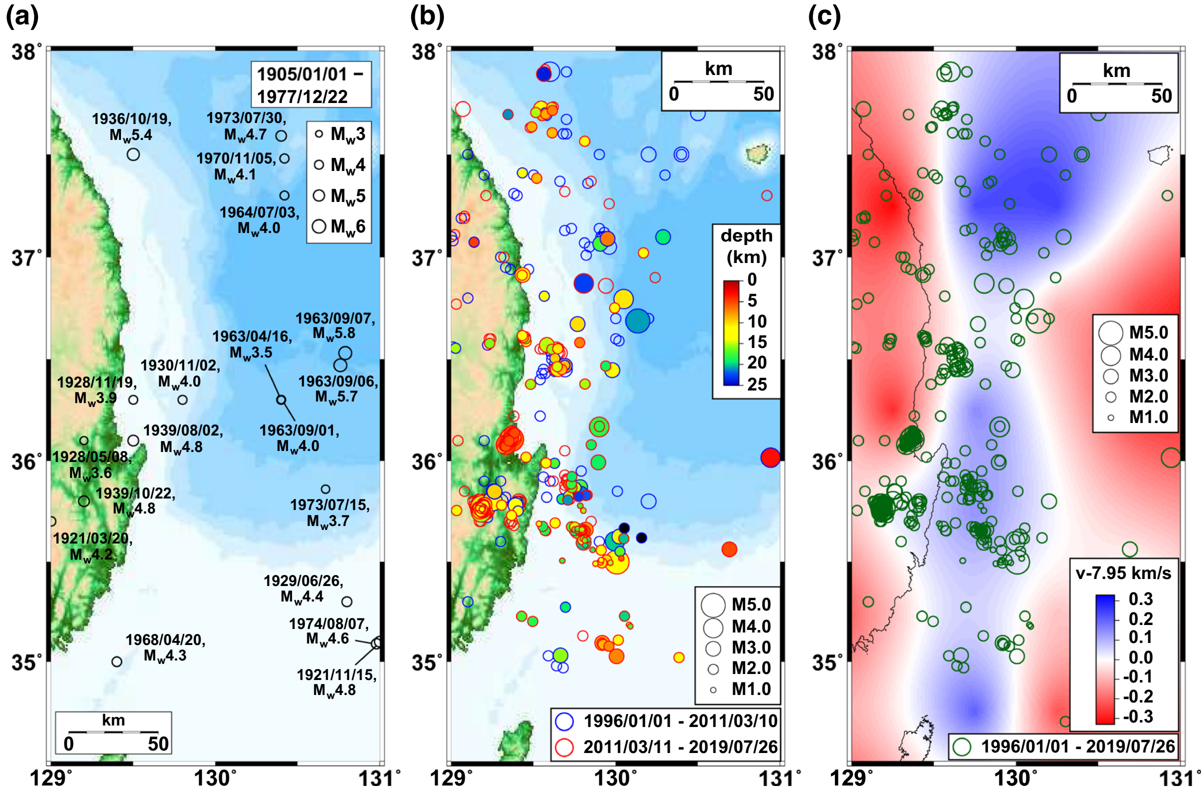

Figure 2

a Instrumental seismicity before 1978, **b** seismicity with focal depths since 1996, and **c** seismicity on the mantle-lid *P*-wave (*Pn*) velocities (Hong and Kang 2009). Some moderate-size earthquakes before 1978 are found inside the Ulleung basin where the seismicity after 1978 is rarely observed. The offshore events are clustered on high *Pn* velocity regions that are adjacent to the coast

mantle-lid *P* velocities around the western East Sea vary highly between 7.65 and 8.25 km/s (Hong and Kang 2009). High mantle-lid *P* velocity anomalies are present along the continental shelf between the southeast coast of the peninsula and the western margin of the Ulleung basin (Fig. 2c). The seismic velocity anomalies may be associated with upper-mantle upwelling during continental rifting and/or lower-crustal magma underplating during uplift process prior to continental breakup (White and McKenzie 1989; Esedo et al. 2012).

The East Sea is under compressional stress field induced by the plate convergence in the regions off the eastern and southern Japanese islands. The primary compression stress field is oriented ENE–WSW in the western East Sea and NW–NE in the eastern East Sea (Lee et al. 2017). The stress field produces spatially heterogeneous earthquake properties. The paleo-rifting structures respond to the current ambient stress field, producing thrust earthquakes.

The Ulleung basin is placed near the east coast of the Korean Peninsula. The paleo-rifting structures are major sources of seismic events in the western East Sea. Reverse faulting and strike-slip faulting earthquakes occur in the western East Sea. The seismicity is low in the northwestern East Sea. Most earthquakes occur in the continental shelf off the southeast coast of the Korean Peninsula. This study focuses on the earthquakes around the continental shelf.

National seismic monitoring of South Korea began in 1978. We collect the source information for earthquakes in the continental margin around the east coast of the Korean Peninsula from Korea Meteorological Administration (KMA), Korea Institute of Geoscience and Mineral Resources (KIGAM) and Japan Meteorological Agency (JMA). The total number of collected earthquakes is 1,121,018 (Fig. 1). The hypocenters of earthquakes in the western East Sea are refined using seismic waveform data for stations deployed by KMA and KIGAM. The focal mechanism solutions of recent earthquakes are determined based on regional seismic records.

The instrumental seismicity before 1978 is collected from earlier studies (Jun and Jeon 2001, 2010) (Fig. 2a). The early instrumental earthquake catalogs may be incomplete. We additionally collect historical earthquake records (Lee and Yang 2006; Houng and Hong 2013; Park and Hong 2016). The historical earthquake records also suffer from catalog incompleteness (Houng and Hong 2013). The focal mechanism solutions of early events were collected from previous studies (Choi et al. 2012; Hong and Choi 2012; Hong et al. 2015; Houng et al. 2016; Hong et al. 2018).

3. Methods

We refine the hypocentral parameters of earthquakes using a joint inversion method, VELHYPO (Kim et al. 2014, 2016). We jointly determine the hypocentral parameters and velocity structures. We decluster the earthquake catalog to remove the aftershocks (Marsan and Lengliné 2008). We determine the Gutenberg-Richter frequency-magnitude relationship for the declustered catalog (Rydelek and Sacks 1989)

$$\log N = a - bM, \tag{1}$$

where a and b are constants, M is the magnitude, and N is the annual number of events with magnitudes greater than or equal to M. We determine the constant a and b using the maximum likelihood method (Aki 1965; Bender 1983; Wiemer and Wyss 2000). We additionally use a least-squares method for the determination of the Gutenberg–Richter frequency-magnitude relationship (Guttorp 1987).

We determine the focal mechanism solutions of earthquakes using a long-period waveform inversion (Dreger and Helmberger 1990; Hong et al. 2015). A global-averaged one-dimensional (1-D) velocity model is applied for the inversion (Kennett et al. 1995). We apply P-polarity analyses to determine the focal mechanism solutions of small-size earthquakes (Snoke 2002).

We calculate the Coulomb stress change, ΔCFS, induced by an earthquake (Toda et al. 2005)

$$\Delta \mathrm{CFS} = \Delta\tau - \mu' \Delta\sigma_n, \tag{2}$$

where $\Delta\tau$ is the shear stress change, μ' is the effective frictional coefficient, and $\Delta\sigma_n$ is the normal stress changes (positive for increased compression). The effective frictional coefficient μ' is set at 0.4 (Hong et al. 2015, 2017b; Nalbant et al. 1998). The ambient compressional stress field is oriented in N77°E, and the strength is 6.5 MPa (Hong et al. 2015, 2017b). The lithospheric Young's modulus is set to be 80 GPa, and the Poisson's ratio to be 0.25 (King et al. 1994; Toda et al. 2005; Hong et al. 2015).

The seismicity density is assessed by smoothing the spatial densities of earthquakes (Houng and Hong 2013)

$$D(x_i) = \sum_{j=1}^{N_c}\left[n_j \cdot \exp\left(\frac{-l_{ij}^2}{2\sigma_c^2}\right)\right] \Big/ \sum_{j=1}^{N_c}\left[\exp\left(\frac{-l_{ij}^2}{2\sigma_c^2}\right)\right], \tag{3}$$

where x_i is the discrete location ith cell, N_c is the number of cells discretizing the medium, n_j $(j = 1, 2, \cdots, N_c)$ is the number of earthquakes in the jth cell, l_{ij} is the epicentral distance between the ith cell and the jth cell, and σ_c is a smoothing coefficient rate that control the width of the Gaussian function. We set σ_c to be 30 km. The seismicity density is normalized for time and area.

We determine the maximum magnitude of earthquakes, $M_{\max}$, using the Tate-Pisarenko method based on the instrumental seismicity catalog (Piarenko et al. 1996; Kijko and Singh 2011)

$$M_{\max} = M_{\max}^{obs} + \left(\frac{1}{n}\right) \cdot \frac{1 - \exp[-\beta(M_{\max} - M_{\min})]}{\beta \exp\left[-\beta(M_{\max}^{obs} - M_{\min})\right]}, \tag{4}$$

where $M_{\max}^{obs}$ is the observed largest earthquake magnitude, $M_{\min}$ is the minimum magnitude that ensures the completeness of earthquake catalog, and n is the number of earthquakes with magnitudes $M \geq M_{\min}$. Also, $\beta = b\ln(10)$, and b is a constant of the Gutenberg–Richter magnitude-frequency relationship. We determine the maximum magnitude using an iteration scheme (Kijko and Singh 2011; Hong et al. 2016b).

The peak ground acceleration (PGA) attenuates with distance. The PGA satisfies a relationship (Atkinson and Boore 1995; Marin et al. 2004; Hong et al. 2016a)

$$\log \mathrm{PGA}_j = A_j + B_j \log r + C_j r, \tag{5}$$

where PGA_j ($j = h, v$) is the horizontal or vertical PGA at the hypocentral distance of r, A_j is a constant calibrated for event size, B_j is a constant for geometrical spreading, and C_j is a constant for anelastic absorption. The PGA is in m/s^2, and the distance r is in km.

The theoretical curve was developed based on the PGAs produced by the earthquakes in the Korean Peninsula (Hong et al. 2016a). Constant A_j is proportional to the body-wave magnitude m_b (Hong et al. 2016a):

$$\begin{aligned} A_h &= -0.318 + 0.394\, m_b, \\ A_v &= -0.273 + 0.372\, m_b. \end{aligned} \tag{6}$$

Constants B_h, B_v, C_h, and C_v are given by $-1.44, -1.54, -0.00211$, and -0.00164 (Hong et al. 2016a). Using the relationships among body-wave magnitude (m_b), moment magnitude (M_w) and seismic moment (M_0) (Kanamori 1977; Hanks and Kanamori 1979; Patton and Walter 1993), we express the PGA attenuation equation as a function of moment magnitude:

$$\begin{aligned} \log \mathrm{PGA}_h &= -0.476 + 0.528\, M_w - 1.44 \log(r) - 0.00211\, r, \\ \log \mathrm{PGA}_v &= -0.422 + 0.498\, M_w - 1.54 \log(r) - 0.00164\, r, \end{aligned} \tag{7}$$

where r is the hypocentral distance in km.

The seismic intensity attenuation equation for the Korean Peninsula is given by (Park and Hong 2017)

$$\begin{aligned} I(M_\mathrm{L}, r) = &-0.998(\pm 0.222) + 1.72(\pm 0.04) M_\mathrm{L} \\ &- 0.644(\pm 0.027) \ln(r) \\ &- 0.00608(\pm 0.00049)\, r, \end{aligned} \tag{8}$$

where I is the seismic intensity in the modified Mercalli intensity (MMI) scale, M_L is the local magnitude, and r is the hypocentral distance in km. Using the relationships among local magnitudes (M_L) and moment magnitude (M_w) (Sheen et al. 2018), the intensity attenuation equation can be written to be

$$I(M_w, r) = -2.49 + 2.02 M_w - 0.644 \ln(r) - 0.00608\, r. \tag{9}$$

4. Seismicity Features

The western East Sea is a major seismic zone around the Korean Peninsula. Most offshore seismicity since 1978 is observed near the eastern coast of the peninsula. The offshore seismicity is low in the northwestern East Sea. The spatial distribution of seismicity illuminates the margins of offshore basins that are associated with paleo-rifting structures. The seismicity is low inside the offshore basins. Most seismicity is clustered in the continental shelf region between the southeast coast of the peninsula and the western margin of the Ulleung basin where high mantle-lid P-wave velocities are observed (Fig. 2c).

The paleo-rifting structure is a major source to spawn offshore earthquakes. Some regions such as Ulsan offshore region display abrupt seismicity increase since the 2011 M_w9.0 Tohoku-Oki megathrust earthquake (Figs. 2b, 3c). Recent seismic activity suggests dominant release of cumulated stress. Notable offshore events include the 15 April 1981 M_w5.2 (M_L4.8) Pohang offshore earthquake, the 29 May 2004 M_w5.0 (M_L5.2) Uljin offshore earthquake, and the 5 July 2016 M_w4.9 (M_L5.0) Ulsan offshore earthquake (Fig. 1b).

The source mechanisms of the earthquakes are mixed with strike slip and reverse faulting (Fig. 3). Strike-slip events occur dominantly in the continental shelf area of the southeastern peninsula. Reverse-faulting earthquakes striking in NS occur along the western margins of the Ulleung basin. These strike-slip and reverse faulting earthquakes are clustered around the Ulleung and Hupo faults (Fig. 3b). The reverse-faulting earthquakes mainly occur around the Ulleung fault, which suggests reverse activation of the paleo-rifting structure in the current compressional stress field (Choi et al. 2012).

We also find strike-slip events around the paleo-rifting structures where reverse activation occurs. This observation suggests neotectonic evolution for

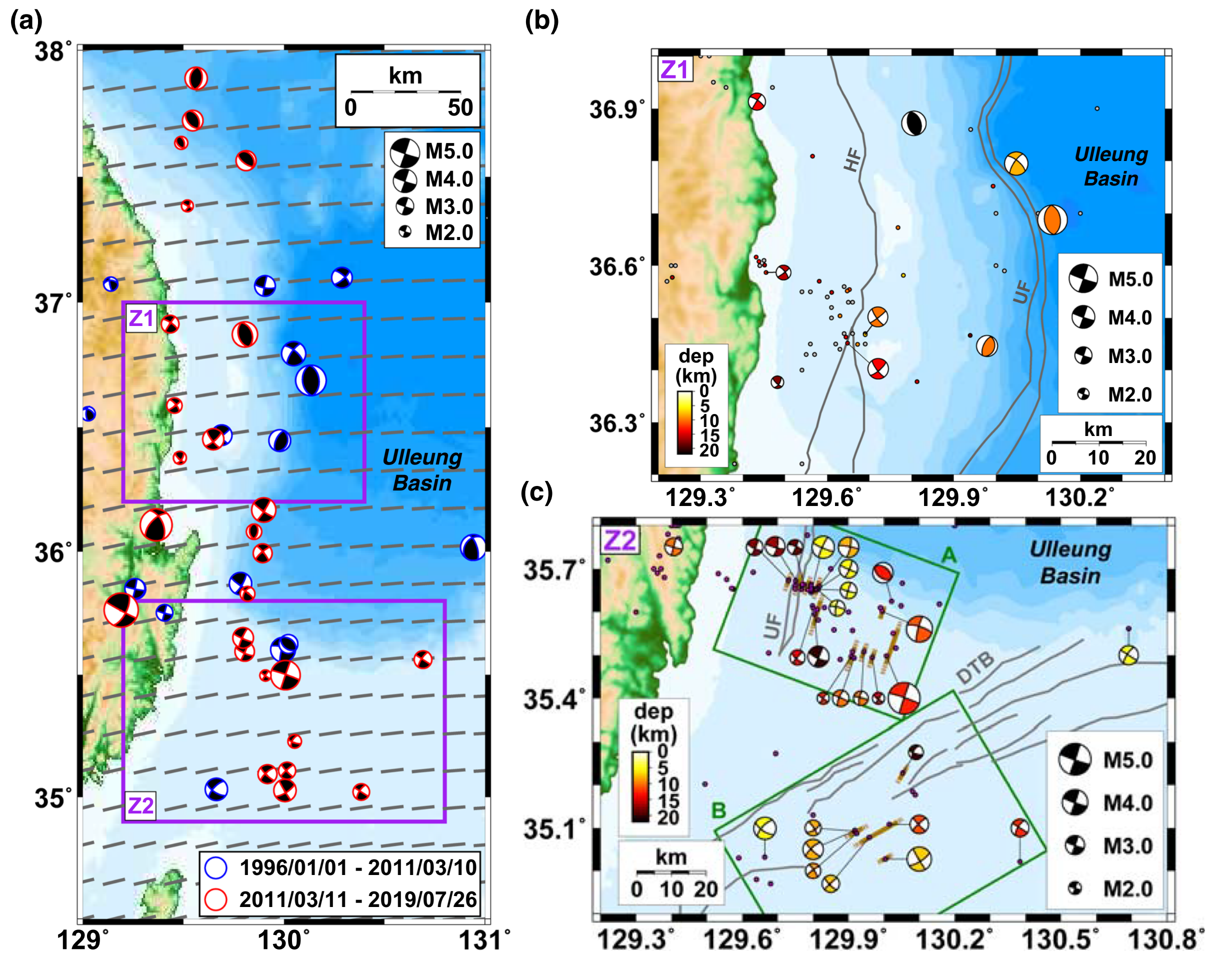

Figure 3

Focal mechanism solutions of earthquakes **a** in the western East Sea, **b** continental shelf area in the vicinity of the midwestern Ulleung basin, and **c** continental shelf area to the southwest of the Ulleung basin. Regions Z1 and Z2 in **a** are enlarged in **b** and **c**. Major fault systems including the Hupo fault (HP), Ulleung fault (UF) and Dolgorae thrust belt (DTB) are indicated. The orientation of the compressional stress field is resented with dotted lines in **a**. Seismicity in the mid-western East Sea is clustered around the Hupo and Ulleung faults. A series of strike-slip faults striking in NNE or NE develop in the southwestern margin of the Ulleung basin (region A). Strike-slip faults striking in ENE develop in the DTB region (region B). Paleo-tectonic structures respond to the current ambient stress field, representing neotectonic motions

the current ambient stress field. The discriminative coseismic and postseismic displacements induced by the megathrust earthquake lowered the yield strength of the medium, which may develop new fault planes or activate paleo-tectonic structures (Choi et al. 2012; Hong et al. 2015). Only the faults optimally-oriented for the current ambient stress field may respond to the stress field.

The neotectonic activity is also found around the southwestern margin of the Ulleung basin (Fig. 3c). We observe strike-slip faults striking in NE in the southwestern margin of the Ulleung basin (region A). The spatial distribution of seismicity in the region suggests a series of subparallel faults develop in the margin of the southwestern Ulleung basin. On the other hand, we observe strike-slip faults striking in ENE in the Dolgorae thrust belt (DTB) region (region B). The strikes of the faults are subparallel with the trend of DTB, suggesting reactivation of thrust belt in

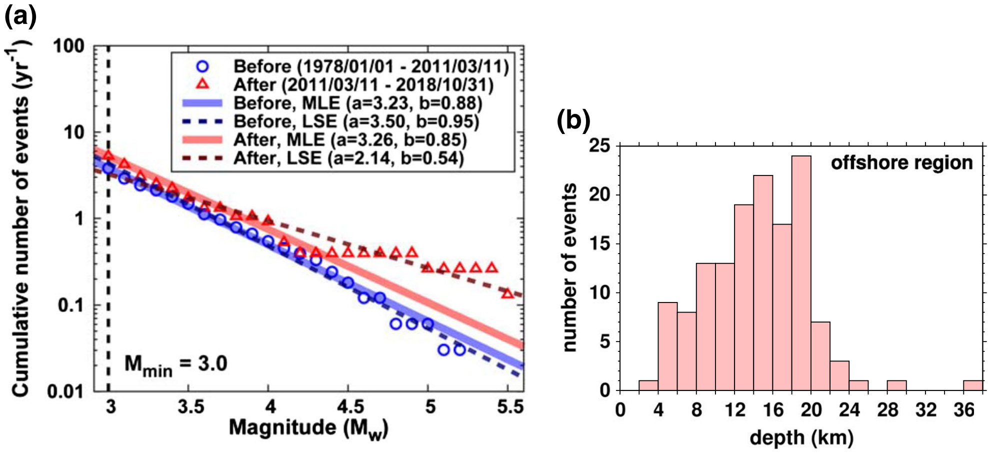

Figure 4

a Gutenberg–Richter frequency-magnitude relationships for seismicity before and after the 2011 M_w9.0 Tohoku-Oki megathrust earthquake, and **b** the distribution of focal depths of offshore events. Apparent increase in moderate-size earthquakes is observed in the seismicity after the megathrust earthquake. The data points are fitted by a maximum likelihood estimation (MLE) and least-squares estimation (LSE). Using the MLE method, the coefficients of the Gutenberg–Richter frequency–magnitude relationship are determined to be comparable for periods before and after the megathrust earthquake. The Gutenberg–Richter frequency–magnitude relationships are determined different for periods before and after the megathrust earthquake using the LSE method. Focal depths are generally distributed between 2 and 30 km, clustering mostly in 12–20 km

strike-slip motion. The paleo-tectonic structures respond to the current ambient stress field.

The focal depths are generally distributed between 2 and 30 km, mostly 12–20 km (Figs. 2b, 4b). The focal depths in the western East Sea are generally deeper than those in the inland regions. The earthquakes in the peninsula have focal depths of 4–20 km, mostly around $\sim$ 5 km (Hong et al. 2016b). However, the 12 September 2016 M_w 5.4 (M_L 5.8) Gyeongju earthquake sequence occurred at depths of 11–16 km (Hong et al. 2017b). The deep focus earthquakes in the western East Sea are unusual considering the crustal thickness. The deep focal depths may be associated with neotectonic activity in the lower crust.

5. *Spatiotemporal Seismicity Change*

We analyze the seismicity changes based on a declustered catalog with the cutoff magnitude of M_w 3.0. We determine the Gutenberg–Richter magnitude–frequency relationships before and after the 2011 M_w 9.0 Tohoku-Oki megathrust earthquake. The b value of the earthquakes before the megathrust earthquake is 0.88 ($\pm$ 0.08), and that of the earthquake after the megathrust earthquake is 0.85 ($\pm$ 0.13) (Fig. 4). The a values are 3.23 ($\pm$ 0.24) and 3.26 ($\pm$ 0.40), suggesting that the yearly occurrence rates of earthquakes with $M_w \geq 0$ are 1700 and 1820 per year.

The a and b values were comparable before and after the megathrust earthquake (Fig. 4). It is noteworthy that the fitting of Gutenberg–Richter frequency–magnitude relationship is poor at large earthquakes for the seismicity after the megathrust earthquake. The Gutenberg–Richter magnitude–frequency relationship for the seismicity before the megathrust earthquake suggests that earthquakes with magnitudes M_w 5.0, 6.0, and 7.0 may occur within every $\sim$ 44, $\sim$ 336, and $\sim$ 2550 years at 95% confidence level.

We additionally determine the Gutenberg–Richter magnitude–frequency relationship using a least-squares method. The b value for the seismicity before the megathrust earthquake is determined consistent. On the other hand, the b value after the megathrust earthquake is lowered. This feature may be because moderate-size earthquake with magnitudes greater than M_w 4.5 increased after the megathrust

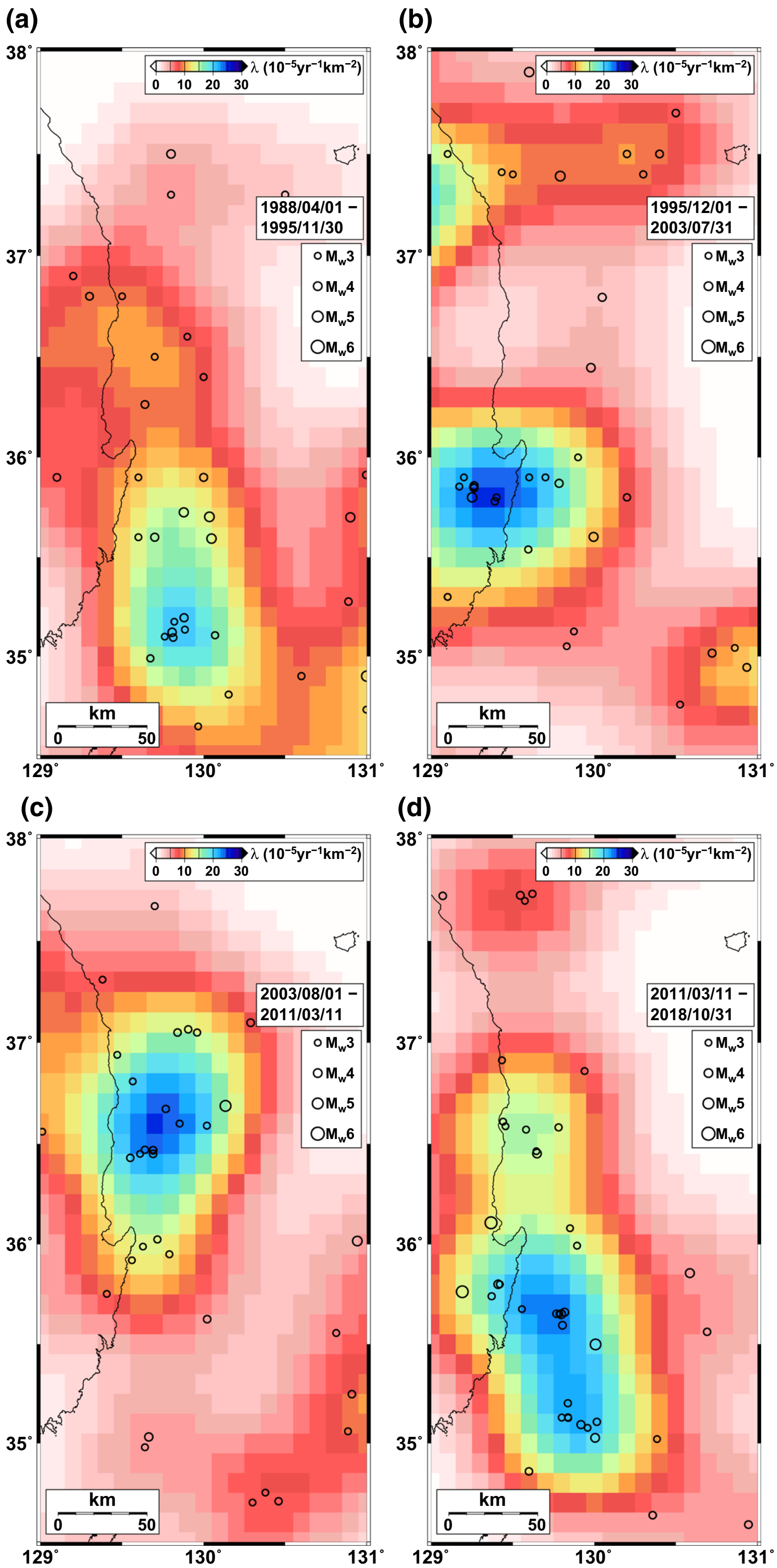

(a)
(b)
(c)
(d)
λ (10⁻⁵yr⁻¹km⁻²)
0 10 20 30
1988/04/01 – 1995/11/30
1995/12/01 – 2003/07/31
2003/08/01 – 2011/03/11
2011/03/11 – 2018/10/31
Mw3
Mw4
Mw5
Mw6
km
0 50
38°
37°
36°
35°
129°
130°
131°

Figure 5
Temporal variation of seismicity densities in the western East Sea: periods of **a** April 1988 to November 1995, **b** December 1995 to July 2003, **c** August 2003 to March 2011, and **d** March 2011 to October 2018. The duration of each time period is $\sim$ 7.6 years. The spatial distribution of seismicity changes with time

earthquake. The observation is consistent with that in the Korean Peninsula (Hong et al. 2018).

We assess the seismicity density for a time period of 7.6 years before and after the 2011 megathrust earthquake (Fig. 5). We observe apparent difference in seismicity distribution before and after the 2011 Tohoku-Oki megathrust earthquake. The seismicity before and after the 2011 Tohoku-Oki megathrust earthquake was spatially separated in most regions. The spatial distribution of seismicity changes with time. The seismicity after the megathrust earthquake increased in regions of low seismicity. The observation suggests that the earthquakes occurred in regions of long-term stress cumulation, lowering the stress level in the medium.

It is intriguing to note that the spatial distribution of seismicity in April 1988 to November 1995 is generally similar to that in March 2011 to October 2018 (Fig. 5). The observation suggests that the seismicity repeats after stress cumulation for a time lapse. The moderate-size earthquake increase after the megathrust earthquake may be associated with the

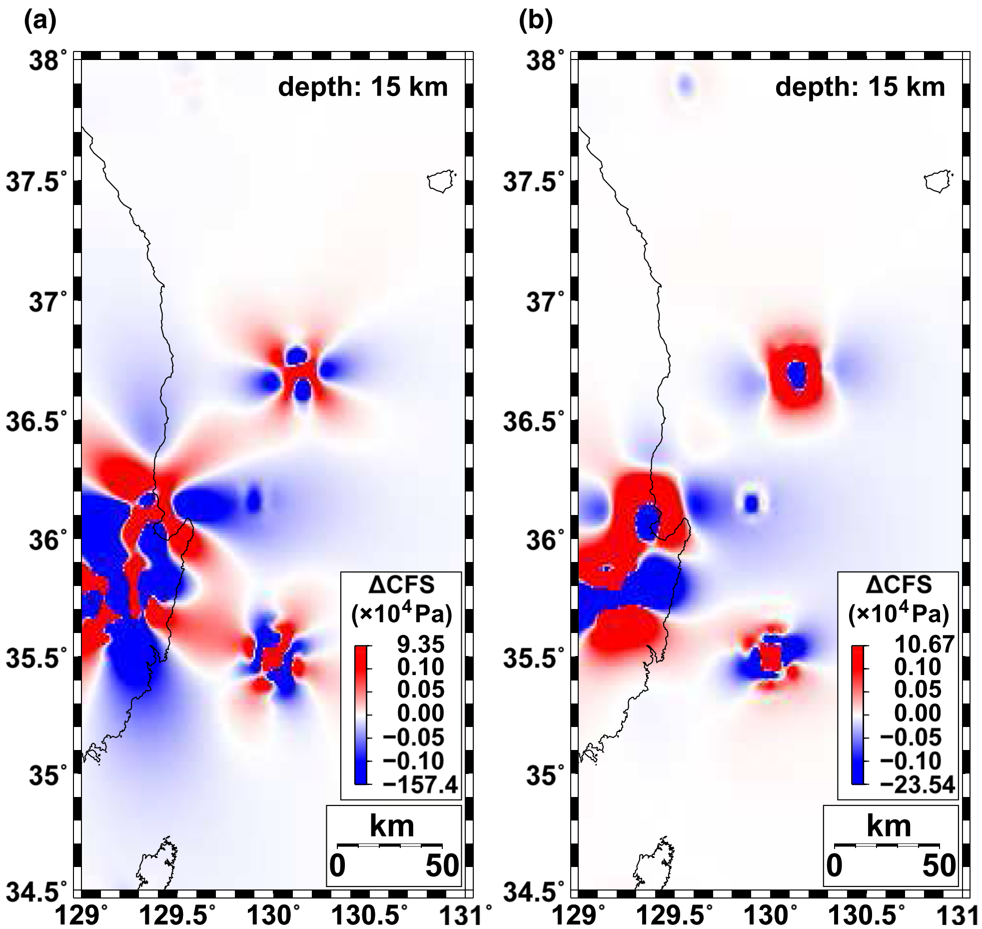

Figure 6
Induced Coulomb stress change by 14 earthquakes with magnitudes $M_L \geq 4.0$ since 2000 for **a** optimally-oriented strike-slip faults and **b** optimally-oriented reverse faults at a depth of 15 km. The inland events produced positive Coulomb stress changes for optimally-oriented strike-slip faults over a southeastern offshore region where recent seismicity is high. The influence of inland events is relatively limited for optimally-oriented reverse faults

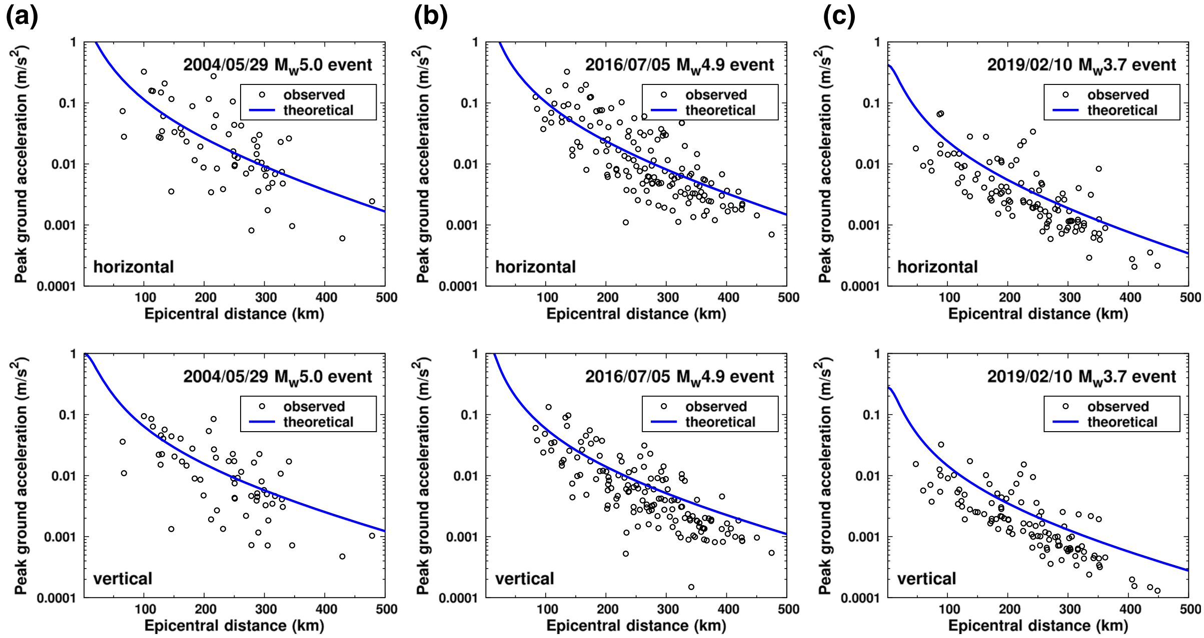

Figure 7

Comparison of observed peak ground accelerations (PGAs) with a theoretical curve in horizontal (upper figures) and vertical components (lower figures) for three representative offshore events: **a** the 29 May 2004 M_w5.0 earthquake, **b** the 5 July 2016 M_w4.9 earthquake, and **c** the 10 February 2019 M_w3.7 earthquake. The observed PGAs match reasonably with the theoretical PGA attenuation curves. The events locations are marked in Fig. 1b

yield strength decrease in the medium. Faults may respond to the differential stress change, producing new fault planes. The characteristic spatiotemporal seismicity changes suggest potential locations of earthquakes that may include regions around the northwestern and northern margins of the Ulleung basin.

6. *Induced Coulomb Stress Changes*

We stack the Coulomb stress changes that were induced by 14 earthquakes with magnitudes greater than or equal to M_L 4.0 since 2000. The cumulative Coulomb stress changes are calculated for optimally-oriented strike-slip and reverse faults at a depth of 15 km (Fig. 6). The cumulative Coulomb stress changes are effective only for local regions. The cumulative Coulomb stress change for the optimally-oriented strike-slip faults reaches the peak positive value of 93 kPa at the region of 35.50° N and 130.00° E. Also, the peak cumulative Coulomb stress change of 107 kPa is observed for the optimally-oriented reverse faults at the region of 35.80° N and 129.20° E.

Recent M5-level events in 2016 and 2017 affect the southeastern region off Pohang (Fig. 1b). The induced stress from the 2016 M_w5.4 (M_L5.8) Gyeongju earthquakes and the 2017 M_w5.5 (M_L5.4) Pohang earthquake may be effective to trigger strike-slip events in the region off the southeastern peninsula, while less to excite thrust events (Fig. 6). The feature agrees with apparent increase in strike-slip events in the southeastern region off Pohang. The 10 February 2019 M_w 3.7 (M_L 4.1) Pohang offshore earthquake occurred in the stress-induced region (Figs. 1b, 6).

The spatiotemporal distribution of seismicity density and Coulomb stress changes suggests potential locations of future earthquakes. Recent seismicity is concentrated in the offshore region in latitudes of 34.7° N–35.7° N, $\sim$36.6° N, and $\sim$37.7° N. The longitudes are 129.4° E–130.5° E. The potential locations are naturally close to the coast. The

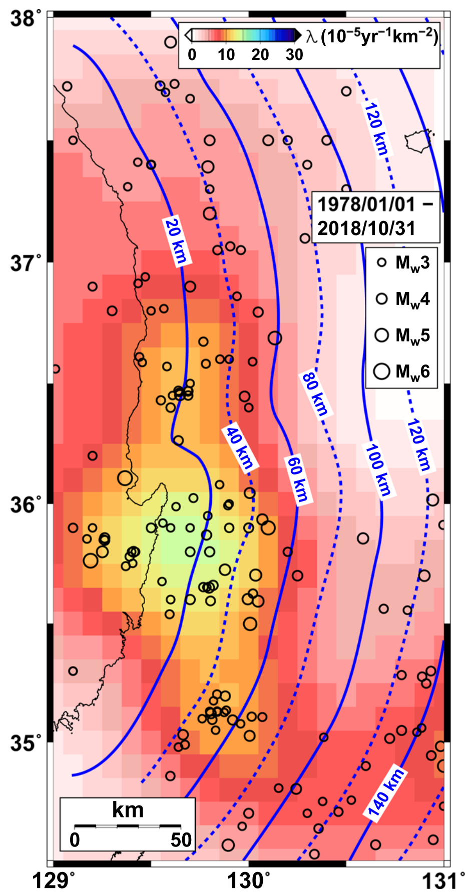

Figure 8
Seismicity distribution of magnitudes $M_w \geq 3.0$ since 1978 and iso-distance lines in the western East Sea. The iso-distance lines presents the distance from the coast. Most seismicity is placed in distances less than 60 km from the coast

earthquakes in latitudes lower than 36° N may be strike-slip events. Both strike-slip and thrust events can occur in latitudes of >36 ° N considering the focal mechanism solutions of precedent events and induced Coulomb stress changes.

7. *Strong Ground Motions*

The instrumental and historical seismicity suggests possible occurrence of large earthquakes (Jun and Jeon 2001; Lee and Yang 2006; Jun and Jeon 2010; Houng and Hong 2013; Park and Hong 2016). The maximum magnitude for earthquakes based on the instrumental seismicity since 1978 is 6.02 from the Tate–Pisarenko method (Piarenko et al. 1996; Kijko and Singh 2011; Hong et al. 2016b), which agrees with the instrumental seismicity before 1978. Further, the instrumental seismicity in regions adjacent to the western East Sea that include the southern Japanese islands presents earthquakes with magnitudes ranging up to 7.0. Strong ground motions by large earthquakes in the western East Sea may produce high damages on coastal regions.

We present the peak ground accelerations (PGAs) of three earthquakes with magnitudes of M_w 3.7, 4.9 and 5.0 at stations in the Korean Peninsula (Fig. 7). The observed PGAs match well with the theoretical PGA attenuation curves at local and near-regional distances. The fitness verifies the PGA attenuation curve for offshore events in the distance less than 250 km. However, we find deviations at distances greater than $\sim$300 km. The theoretical curve overestimates the PGA levels at large distances. The poor fitness at large distances may be partly due to the presence of laterally heterogeneous crustal structures in the East Sea that induce increasing seismic attenuation with distance.

The instrumental seismicity presents that most earthquakes occur in distances less than $\sim$ 60 km from the east coast of the peninsula (Fig. 8). We assess possible levels of strong ground motions for major earthquakes with magnitudes of M_w 6.0, 6.5, and 7.0 and three representative focal depths of 5, 10, and 15 km. The earthquakes with focal depth of 5 km may produce a horizontal PGA of 0.2 g (1.96 m/s^2) at distances of 39, 57, and 81 km (Fig. 9). The vertical PGA reaches 0.2 g at distances of 26, 38, and 54 km. When the earthquakes occur at a focal depth of 15 km, we observe the horizontal PGA of 0.2 g at distances of 38, 56, and 80 km. The vertical PGA of 0.2 g appears at distances of 24, 37, and 53 km. These earthquakes produce the seismic intensities of MMI 6–7, 7–8, and 8–9 at a distance of 60 km (Fig. 10).

8. *Discussion and Conclusions*

The East Sea is a unique place with paleo-rifting structures that respond seismically to the current ambient stress field. The paleo-rifting structures are suited near the east coast of the Korean Peninsula. Strike-slip and thrust earthquakes are dominant in the

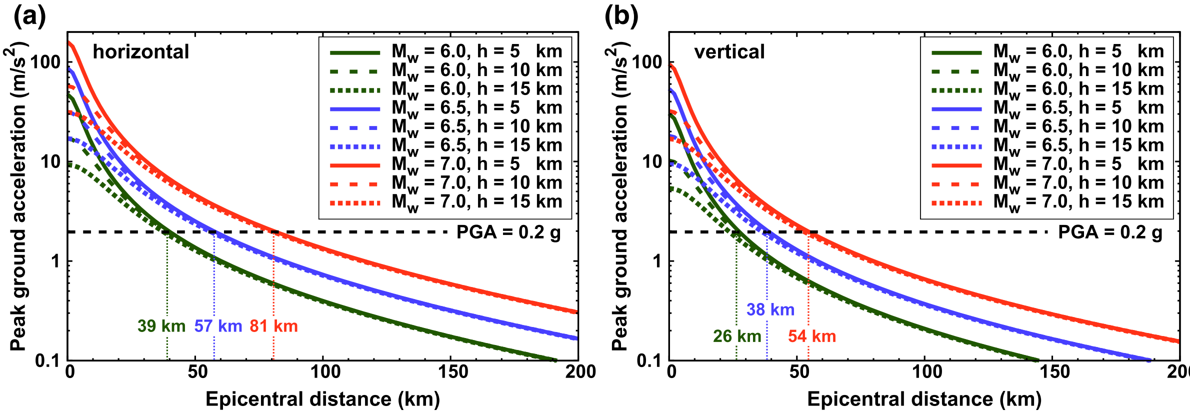

Figure 9
Peak ground acceleration (PGA) attenuation curves in **a** horizontal and **b** vertical components. Cases of three magnitudes (M_w =6.0, 6.5 and 7.0) and three focal depths (h =5, 10, and 15 km) are considered. The PGA level of 0.2 g is indicated. The horizontal PGAs are higher than the vertical PGAs. The horizontal PGA of 0.2 g is expected at distances of 39, 57, and 81 km for events of M_w6.0, 6.5, and 7.0 and $h = 5$ km. The vertical PGA of 0.2 g is found at 26, 38, and 54 km

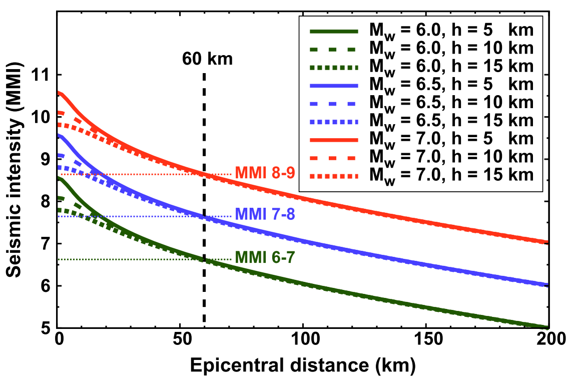

Figure 10
Seismic intensity attenuation curves for three magnitudes (M_w6.0, 6.5, 7.0) and three focal depths (h = 5, 10, 15 km). The seismic intensity is presented in MMI scale. The seismic intensity for events with M_w6.0, 6.5, and 7.0 may reach MMI 6–7, 7–8, and 8–9 at an epicentral distance of 60 km

continental shelf off the east coast of the peninsula. The thrust events suggest that the paleo-rifting structures are reversely activated by the current ambient stress field. On the other hand, the strike-slip events occur in faults that developed by the current stress field.

The low stress cumulation rate causes apparent spatiotemporal migration of seismicity. Large earthquakes may occur with long recurrence intervals. The background seismicity suggests that earthquakes with magnitudes M_w 5.0, 6.0, and 7.0 may occur within every ∼ 44, ∼ 336, and ∼ 2550 years at 95 % confidence level according to the Gutenberg–Richter frequency–magnitude relationship.

The distance-dependent coseismic and postseismic displacements by the 2011 Tohoku-Oki megathrust earthquake perturbed the crustal media in local and regional distances. Local moderate-size earthquakes additionally disturbed the local stress fields. The subsequent perturbation in media and stress field caused a temporal burst of major earthquakes in the western East Sea. Moderate-size earthquakes increased after the megathrust earthquake. Offshore events such as the 10 February 2019 M_w 3.7 (M_L 4.1) Pohang offshore earthquake occurred in a region where the stress was transferred from the inland moderate-size events including the 12 September 2016 M_w5.4 (M_L 5.8) Gyeongju earthquake and 15 November 2017 M_w5.5 (M_L 5.4) Pohang earthquake. The transferred stress and medium perturbations may incur other moderate-size or large earthquakes (Hong et al. 2018).

The focal depths of the earthquakes in the western East Sea are distributed between 2 and 30 km, mostly 12–20 km. These focal depths are generally larger than those of inland events in the Korean Peninsula. The offshore events naturally occur close to the east coast of the peninsula. Large offshore earthquakes may produce strong ground motions around the coast.

The horizontal PGAs are expected to be larger than vertical PGAs. The horizontal PGA of 0.2 g may occur at distances of $\sim$ 40–80 km for earthquakes with magnitudes of M_w 6.0–7.0 and focal depths of 5–15 km. The observation suggests that a large offshore earthquake may produce strong ground motions and damage around the coastal regions.

Acknowledgements

We are grateful to two anonymous reviewers and the editor, Professor Andrzej Kijko for fruitful comments. This work was supported by the Korea Meteorological Administration Research and Development Program under grant KMI2018-02910. Additionally, this research was partly supported by the Basic Science Research Program through the National Research Foundation of Korea (NRF), which is funded by the Ministry of Education (NRF-2017R1A6A1A07015374, NRF-2018R1D1A1A09083446).

Publisher's Note Springer Nature remains neutral with regard to jurisdictional claims in published maps and institutional affiliations.

References

Aki, K. (1965). Maximum likelihood estimate of b in the formula $\log N = a - bM$ and its confidence limits. *Bulletin of the Earthquake Research Institute, Tokyo University*, *43*, 237–239.

Atkinson, M., & Boore, D. M. (1995). Ground-motion relations for eastern North America. *Bulletin of the Seismological Society of America*, *85*, 17–30.

Bender, B. K. (1983). Maximum likelihood estimation of b values for magnitude grouped data. *Bulletin of the Seismological Society of America*, *73*(3), 831–851.

Chang, S.-J., & Baag, C.-E. (2006). Crustal structure in southern Korea from joint analysis of regional broadband waveforms and travel times. *Bulletin of the Seismological Society of America*, *96*, 856–870.

Choi, H., Hong, T.-K., He, X., & Baag, C.-E. (2012). Seismic evidence for reverse activation of a paleo-rifting system in the East Sea (Sea of Japan). *Tectonophysics*, *572–573*, 123–133.

Chough, S. K., Kwon, S.-T., Ree, J.-H., & Choi, D. K. (2000). Tectonic and sedimentary evolution of the Korean peninsula: a review and new view. *Earth-Science Reviews*, *52*, 175–235.

Dreger, D. S., & Helmberger, D. V. (1990). Broadband modeling of local earthquakes. *Bulletin of the Seismological Society of America*, *80*, 1162–1179.

Esedo, R., van Wijk, J., Coblentz, D., & Meyer, R. (2012). Uplift prior to continental breakup: Indication for removal of mantle lithospehre? *Geosphere*, *8*, 1078–1085.

Fitches, W. R., Fletcher, C. J. N., & Xu, J. (1991). Geotectonic relationships between cratonic blocks in E. China and Korea. *Journal of Southeast Asian Earth Sciences*, *6*, 185–199.

Furumura, T., Hong, T.-K., & Kennett, B. L. N. (2014). Lg wave propagation in the area around Japan: Observations and simulations. *Progress in Earth and Planetary Science*, *1*, 10. https://doi.org/10.1186/2197-4284-1-10.

Guttorp, P. (1987). On least-squares estimation of b values. *Bulletin of the Seismological Society of America*, *77*(6), 2115–2124.

Hanks, T. C., & Kanamori, H. (1979). A moment magnitude scale. *Journal of Geophysical Research*, *84*, 2348–2350.

Hirata, N., Karp, B. Y., Yamaguchi, T., Kanazawa, T., Suyehiro, K., Kasahara, J., et al. (1992). Oceanic crust in the Japan Basin of the Japan Sea by the 1990 Japan-USSR expedition. *Geophysical Research Letters*, *19*, 2027–2030.

Hong, T.-K. (2010). Lg attenuation in a region with both continental and oceanic environments. *Bulletin of the Seismological Society of America*, *100*(2), 851–858.

Hong, T.-K., Baag, C.-E., Choi, H., & Sheen, D.-H. (2008). Regional seismic observations of the October 9, 2006 underground nuclear explosion in North Korea and the influence of crustal structure on regional phases. *Journal of Geophysical Research*, *113*, B03305. https://doi.org/10.1029/2007JB004950.

Hong, T.-K., & Choi, H. (2012). Seismological constraints on the collision belt between the North and South China blocks in the Yellow Sea. *Tectonophysics*, *570–571*, 102–113.

Hong, T.-K., Choi, E., Park, S., & Shin, J. S. (2016a). Prediction of ground motion and dynamic stress change in Baekdusan (Changbaishan) volcano caused by a North Korean nuclear explosion. *Scientific Reports*, *6*, 21477. https://doi.org/10.1038/srep21477.

Hong, T.-K., & Kang, T.-S. (2009). Pn travel-time tomography of the paleo-continental-collision and rifting zone around Korea and Japan. *Bulletin of the Seismological Society of America*, *99*(1), 416–421.

Hong, T. K., & Lee, K. (2012). m_b(Pn) Scale for the Korean Peninsula and Site-Dependent Pn Amplification. *Pure and Applied Geophysics*, *169*, 1963–1975.

Hong, T.-K., Lee, J., Chi, D., & Park, S. (2017a). Seismic velocity changes in the backarc continental crust after the 2011 Mw 9.0 Tohoku-Oki megathrust earthquake. *Geophysical Research Letters*, *44*, 10997–11003. https://doi.org/10.1002/2017GL075447.

Hong, T. K., Lee, J., & Houng, S. E. (2015). Long-term evolution of intraplate seismicity in stress shadows after a megathrust. *Physics of the Earth and Planetary Interiors*, *245*, 59–70.

Hong, T.-K., Lee, J., Kim, W., Hahm, I.-K., Woo, N. C., & Park, S. (2017b). The 12 September 2016 M_L5.8 mid-crustal earthquake in the Korean Peninsula and its seismic implications. *Geophysical Research Letters*, *44*, 3131–3138. https://doi.org/10.1002/2017GL072899.

Hong, T.-K., Lee, J., Park, S., & Kim, W. (2018). Time-advanced occurrence of moderate-size earthquakes in a stable intraplate region after a megathrust earthquake and their seismic properties. *Scientific Reports*, *8*, 13331. https://doi.org/10.1038/s41598-018-31600-5.

Hong, T. K., Park, S., & Houng, S. E. (2016b). Seismotectonic properties and zonation of the far-eastern Eurasian plate around the Korean Peninsula. *Pure and Applied Geophysics*, *173*, 1175–1195.

Houng, S. E., & Hong, T. K. (2013). Probabilistic analysis of the Korean historical earthquake records. *Bulletin of the Seismological Society of America*, *103*, 2782–2796.

Houng, S. E., Lee, J., & Hong, T. K. (2016). Dynamic seismic response of a stable intraplate region to a megathrust earthquake. *Tectonophysics*, *689*, 67–78.

Jolivet, L., Tamaki, K., & Fournier, M. (1994). Japan Sea, opening history and mechanism: a synthesis. *Journal of Geophysical Research*, *99*, 22237–22259.

Jun, M.-S., & Jeon, J.-S. (2001). Early instrumental earthquake data (1905–1942) in Korea. *Economic and Environmental Geology*, *34*(6), 573–581.

Jun, M.-S., & Jeon, J.-S. (2010). Focal mechanism in and around the Korean peninslua. *Jigu-Mulli-wa-Tamsa*, *13*(3), 198–202.

Kanamori, H. (1977). The energy release in great earthquakes. *Journal of Geophysical Resarch*, *82*, 2981–2987.

Kennett, B. L. N., Engdahl, E. R., & Buland, R. (1995). Constraints on seismic velocities in the Earth from traveltimes. *Geophysical Journal International*, *122*, 108–124.

Kijko, A., & Graham, G. (1998). Parametric-historic procedure for probabilistic seismic hazard analysis. Part I: Estimation of maximum regional magnitude m_{max}. *Pure and Applied Geophysics*, *152*, 413–442.

Kijko, A., & Singh, M. (2011). Statistical tools for maximum possible earthquake magnitude estimation. *Acta Geophysica*, *59*(4), 674–700.

Kim, H.-J., Han, S.-J., Lee, G. H., & Huh, S. (1998). Seismic study of the Ulleung Basin crust and its implications for the opening of the East Sea (Japan Sea). *Marine Geophysical Researches*, *20*, 219–237.

Kim, W., Hong, T.-K., & Kang, T. S. (2014). Hypocentral parameter inversion for regions with poorly known velocity structures. *Tectonophysics*, *627*, 182–192.

Kim, W., Hong, T.-K., Lee, J., & Taira, T. A. (2016). Seismicity and fault geometry of the San Andreas fault around Parkfield, California and their implications. *Tectonophysics*, *677*, 34–44.

Kim, Y.-S., Jin, K., Choi, W.-H., & Kee, W.-S. (2011). Understanding of active faults: A review for recent researches. *Journal of the Geological Society of Korea*, *47*(6), 723–752.

Kim, H.-J., Jou, H.-T., Cho, H.-M., Bijwaard, H., Sato, T., Hong, J.-K., et al. (2003). Crustal structure of the continental margin of Korea in the East Sea (Japan Sea) from deep seismic sounding data: evidence for rifting affected by the hotter than normal mantle. *Tectonophysics*, *364*, 25–42.

Kim, H.-J., Jou, H.-T., & Lee, G. H. (2018). Neotectonics of the Eastern Korean Margin Inferred from Back-arc Rifting Structure. *Ocean Science Journal*, *53*(3), 601–609.

King, G. C. P., Stein, R. S., & Lin, J. (1994). Static stress changes and the triggering of earthquakes. *Bulletin of the Seismological Society of America*, *84*, 935–953.

Lee, J., Hong, T.-K., & Chang, C. (2017). Crustal stress field perturbations in the continental margin around the Korean Peninsula and Japanese islands. *Tectonophysics*, *718*, 140–149.

Lee, K., & Yang, W. S. (2006). Historical seismicity of Korea. *Bulletin of the Seismological Society of America*, *96*(3), 846–855.

Marin, S., Avouac, J.-P., Nicolas, M., & Schlupp, A. (2004). A probabilistic approach to seismic hazard in metropolitan France. *Bulletin of the Seismological Society of America*, *94*, 2137–2163.

Marsan, D., & Lengliné, O. (2008). Extending earthquakes' reach through cascading. *Science*, *319*, 1076–1079.

Nalbant, S. S., Hubert, A., & King, G. C. (1998). Stress coupling between earthquakes in northwest Turkey and the north Aegean Sea. *Journal of Geophysical Research*, *103*, 24469–24486.

Otofuji, Y.-I., Matsuda, T., & Nohda, S. (1985). Opening mode of the Japan Sea inferred from the palaeomagnetism of the Japan Arc. *Nature*, *317*, 603–604.

Park, S., & Hong, T. K. (2016). Joint determination of event epicenter and magnitude from seismic intensities. *Bulletin of the Seismological Society of America*, *106*, 499–511.

Park, S., & Hong, T.-K. (2017). Regional seismic intensity anomalies in the Korean Peninsula and its implications for seismic-hazard potentials. *Pure and Applied Geophysics*, *174*(7), 2561–2579.

Patton, H. J., & Walter, W. R. (1993). Regional moment: magnitude relations for earthquakes and explosions. *Geophysical Research Letter*, *20*, 277–280.

Pisarenko, V. F., Lyubushin, A. A., Lysenko, V. B., & Golubieva, T. V. (1996). Statistical estimation of seismic hazard parameters: Maximum possible magnitude and related parameters. *Bulletin of the Seismological Society of America*, *86*, 691–700.

Rydelek, P. A., & Sacks, I. S. (1989). Testing the completeness of earthquake catalogues and the hypothesis of self-similarity. *Nature*, *337*, 251–253.

Sheen, D. H., Kang, T. S., & Rhie, J. (2018). A local magnitude scale for South Korea. *Bulletin of the Seismological Society of America*, *108*, 2748–2755.

Snoke, J. A. (2002). FOCMEC: FOcal MEChanism determinations. In W. H. K. Lee, H. Kanamori, P. C. Jennings, & C. Kisslinger (Eds.), *International Handbook of Earthquake and Engineering Seismology, Part B* (pp. 1629–1630). San Diego: Academic Press.

Toda, S., Stein, R. S., Richards-Dinger, K., & Bozkurt, S. B. (2005). Forecasting the evolution of seismicity in southern California: Animations built on earthquake stress transfer. *Journal of Geophysical Research*, *110*, B05S16. https://doi.org/10.1029/2004JB003415.

White, R., & McKenzie, D. (1989). Magmatism at rift zones: the generation of volcanic continental margins and flood basalts. *Journal of Geophysical Research*, *94*(B6), 7685–7729.

Wiemer, S., & Wyss, M. (2000). Minimum magnitude of completeness in earthquake catalogs: Examples from Alaska, the Western United States, and Japan. *Bulletin of the Seismological Society of America*, *90*, 859–869.

Yin, A., & Nie, S. (1993). An indentation model for the north and south China collision and development of the Tan-Lu and Honam fault systems, eastern Asia. *Tectonics*, *12*, 810–813.

Yoon, S. H., Sohn, Y. K., & Chough, S. K. (2014). Tectonic, sedimentary, and volcanic evolution of a back-arc basin in the East Sea (Sea of Japan). *Marine Geology*, *352*, 70–88.

(Received November 23, 2019, revised March 11, 2020, accepted March 31, 2020, Published online April 21, 2020)